ELSEVIER

Medical Engineering & Physics 25 (2003) 259–274

Medical Engineering & Physics

www.elsevier.com/locate/medengphy

Kinematics of the human pelvis following open book injury

M.S. Hefzy [a,b,*], N. Ebraheim [b], A. Mekhail [c], D. Caruntu [a], H. Lin [a], R. Yeasting [d]

[a] *Biomechanics and Assistive Technology Laboratory, Department of Mechanical, Industrial and Manufacturing Engineering, The University of Toledo, Toledo, Ohio 43606, USA*

[b] *Department of Orthopaedic Surgery, The Medical College of Ohio, Toledo, Ohio 43699, USA*

[c] *Department of Orthopaedic Surgery, Cleveland Clinic Foundation, Cleveland, Ohio 44195, USA*

[d] *Department of Anatomy, The Medical College of Ohio, Toledo, Ohio 43699, USA*

Received 30 January 2002; received in revised form 28 August 2002; accepted 15 October 2002

Abstract

The objective of this study is to determine the three dimensional kinematics of the human pelvis including both sacroiliac joints following a simulated open book injury induced on cadavers by applying anterior-posterior compressive loads to the pelvis. An electromagnetic digitizing and motion tracking system was utilized to measure the morphology of the pelvis and the relative movements of its bones during this simulated open book fracture. The screw displacement axis method was used to describe the relative motion between the sacrum and each hipbone.

Morphologically, it was found that the articular surfaces forming the sacroiliac joints could be approximated with planar surfaces directed from proximal and lateral to distal and medial and from posteromedial to anterolateral. The kinematic data obtained from this study indicate that there is a direct correlation between the opening of the symphysis pubis and the opening of the sacroiliac joint (SIJ) during open book injury. This suggests that the extent of injury of the SIJ maybe estimated from the degree of opening of the symphysis pubis as demonstrated on anteroposterior (A–P) x-rays. The results obtained from this study also indicate that the motion of the hipbone with respect to the sacrum on the side of the sacroiliac joint opening is almost a pure rotation, which translates clinically on the A–P x-rays as pure opening of the SIJ without vertical displacement. The average axis of rotation was found to be almost parallel to the SIJ planar articular surface. Furthermore, the pubic bone on the side of SIJ opening was found to displace inferiorly and posteriorly. One can thus conclude that in open book pelvic injuries, the pubic bone on the side of injury displaces inferiorly on the outlet projection x-rays with no vertical displacement of the SIJ. This is important since the initial assessment of the open book injury in the emergency room includes outlet projection x-rays. From this study, the relative vertical positions of the pubic bones on these x-rays can help the surgeon in differentiating open book fracture injury from other pelvic injuries.

Keywords: Human pelvis; Open book injury; Kinematics

1. Introduction

The management of traumatic disruption of the pelvic ring has become a focus of interest because it has significant consequences in the form of both death and disability. Tile [1] reported that the mortality of major pelvic fractures continue to be about 10%. He also indicated that pelvic injury is found in 12% of victims expiring after excessive blunt trauma, in 22% of fatal accidents and in 45% of fatal accidents to pedestrians.

Proper management of pelvic ring injuries requires an in-depth understanding of the anatomy of the pelvis, its biomechanics, and the mechanisms of injury. By understanding these, and with precise clinical and radiographic evaluation of the injury, appropriate management and treatment can be chosen. This is critical since an inappropriate treatment can create significant problems for a functional recovery following trauma. Only a few biomechanical reports have been published to describe the mechanisms and the principles of treatment of the skeletal injury and the eventual functional outcomes.

* Corresponding author. Tel.: +1-419-530-8234; fax: +1-419-530-8206.

E-mail address: mhefzy@eng.utoledo.edu (M.S. Hefzy).

1350-4533/03/$30.00 © 2003 IPEM. Published by Elsevier Science Ltd. All rights reserved.
doi:10.1016/S1350-4533(02)00196-0

Nomenclature

$\mathbf{R}_P$, $\mathbf{r}_P$ position vectors of any point with respect to (hereafter w.r.t.) the source coordinate system located on the left ilium and the sacrum (global) bony coordinate system, respectively;
$\mathbf{r}_{li-so}$ position vector of any point on the left ilium w.r.t. the source coordinate system;
$\mathbf{r}_{ri-so}$ position vector of any point on the right ilium w.r.t. the source coordinate system;
$\mathbf{r}_{sc-so}$ position vector of any point on the sacrum w.r.t. the source coordinate system;
$\mathbf{r}_{ri-ri}$ position vector of any point on the right ilium w.r.t. the sensor coordinate system on the right ilium;
$\mathbf{r}_{sc-sc}$ position vector of any point on the sacrum w.r.t. the bony coordinate system on the sacrum;
$(\mathbf{r}_{ri-bsc})_2$ position vector of any point on the right ilium w.r.t. the bony coordinate system on the sacrum at an arbitrary position, position 2;
$(\mathbf{r}_{li-bsc})_2$ position vector of any point on the left ilium w.r.t. the bony coordinate system on the sacrum at an arbitrary position, position 2;
$(\mathbf{r}_{sc-bsc})_2$ position vector of any point on the sacrum w.r.t. the bony coordinate system on the sacrum at an arbitrary position, position 2;
$(\mathbf{r}_{sc-so})_d$ position vector of any point on the sacrum w.r.t. the source coordinate system at the position of digitization;
$(\mathbf{r}_{sc-so})_2$ position vector of any point on the sacrum w.r.t. the source coordinate system at an arbitrary position, position 2;
$(\mathbf{r}_{ri-so})_2$ position vector of any point on the right ilium w.r.t. the source coordinate system at an arbitrary position, position 2;
$[R_{SOBSC}]$ 3 x 3 rotational matrix from the source coordinate system to the sacrum bony coordinate system;
$[R_{SRILSO}]$ 3×3 rotational matrix from the sensor coordinate system on the right ilium to the source coordinate system;
$[R_{SSCSO}]$ 3×3 rotational matrix from the sensor coordinate system on the sacrum to the source coordinate system;
$[B_{SOSSC}]$ 4×4 transformation matrix from the source coordinate system to the sensor system located on the sacrum;
$[B_{SOSSC}]_2$ 4×4 transformation matrix from the source coordinate system to the sensor system located on the sacrum at position 2;
$[B_{SOSSC}]_d$ 4×4 transformation matrix from the source coordinate system to the sensor system located on the sacrum at the position of digitization;
$[B_{SSCSO}]$ 4×4 transformation matrix from the sensor coordinate system on the sacrum to the source coordinate system $\{=[B_{SOSSC}]^{-1}\}$;
$[B_{SOBSC}]$ 4×4 transformation matrix from the source coordinate system to the sacrum bony coordinate system;
$[B_{BSCSO}]$ 4×4 transformation matrix from the sacrum bony coordinate system to the source coordinate system $\{=[B_{SOBSC}]^{-1}\}$;
$[B_{SOSRIL}]$ 4×4 transformation matrix from the source coordinate system to the sensor system located on the right ilium;
$[B_{SRILSO}]$ 4×4 transformation matrix from the sensor system located on the right ilium to the source coordinate system $\{=[B_{SOSRIL}]^{-1}\}$;
$[B_{BSCSSC}]$ 4×4 transformation matrix from the bony coordinate system on the sacrum to the sensor system located on the sacrum;
$[B_{SSCBSC}]$ 4×4 transformation matrix from the sensor system located on the sacrum to the bony coordinate system on the sacrum $\{=[B_{BSCSSC}]^{-1}\}$;
$[B]_{1-2}$ 4×4 transformation matrix describing the motion of a moving body w.r.t. a fixed body from position 1 to position 2;
$[B_{1-2}]_1$, $[B_{1-2}]_2$ 4×4 transformation matrices describing the location of moving body 1 w.r.t. fixed body 2 at positions 1 and 2, respectively;
(l, m, n) direction cosines of the screw axis w.r.t. a system of axes attached to the fixed body;
(x_o, y_o, z_o) coordinates of any point on the screw axis w.r.t. a system of axes attached to the fixed body;
σ, p rotation about and translation along the screw axis, respectively.Subscripts
SO source coordinate system;

BSC	bony sacrum coordinate system;
SRIL	sensor coordinate system located on the right ilium;
SSC	sensor coordinate system located on the sacrum.

Drerup and Hierholzer [2] reported that angular movements of the dimple line could be correlated with the tilt of the pelvis. Gautsch, et al. [3] proposed to use the 3D displays of 3D reconstructed CT scans to facilitate preoperative plans in managing fractures of the pelvis and acetabulae. Major and Helms [4] used radiographic imaging to establish a relation between pubic stress injury and degenerative changes in the sacroiliac joints. Literature review indicates that most studies directed toward understanding the biomechanics of the pelvis were focused on the analysis of side impact to design crash dummies and human body surrogates [5] and side door padding [6]. Renaudin, et al. [7] presented a 3-D finite element model to determine the response of the human pelvis under lateral loading. However, their model was limited in that they assumed no relative movement between the sacrum and the two iliac fossae. Dawson, et al. [8] presented another 3-D finite element model to describe the isolated structural behavior of the pelvis in lateral impact. The model developed by Hoek van Dijke, et al. [9] allowed to analyze the load transfer through the pelvis in static postures when studying low back pain.

This work is directed toward providing an understanding of the biomechanics of the human pelvis, and its mechanisms of injury. Three major classifications for pelvic ring disruptions have been developed and utilized by orthopedic surgeons in assessing patients. The first classification is based on the site of injury and was developed by Judet et al. [10]. The second classification is based on the mechanism of injury and was developed by Young and Burgess [11]. The third classification combines both mechanism of injury and stability and was developed by Tile [1]. Tile indicates that the history of a pelvic fracture depends upon the stability of the injury, among other factors. While stable injuries give few major long-term problems, unstable injuries continue to be problematic. The stability of the pelvic ring depends upon the integrity of the posterior weight-bearing sacroiliac complex, with the major sacroiliac, sacrotuberous and sacrospinous ligaments.

In Young and Burgess [11] classification, three modes of failure are identified: anteroposterior compression injury, lateral compression injuries and vertical shear injury. In the first mode of failure, injury results from an anteroposteriorly directed force producing sacroiliac joint opening, which causes external rotation of the hemi pelvis. In the second mode of failure, injury results from a force parallel to the trabeculae of the sacrum and applied to the lateral aspect of the pelvis. Different lateral compression injuries are found depending on the anteroposterior location of this lateral impacting force. In the third mode of failure, injury results from a vertically directed force causing fracture of the pubic rami and disruption of all the ligamentous structures. Young and Burgess' three-patterns classification has the advantage of alerting the surgeon to potential resuscitation problems associated with pelvic fractures and allow appropriate surgical decision.

This project focuses on anteroposterior injuries, which usually involve pedestrians and motorcyclists and are usually seen in Motor Vehicle Accidents (MVA). Specifically, open book injury of the pelvis is a common anteroposterior injury that is often encountered in MVA. However, the mechanics of this injury is still not fully understood. This particular injury occurs at different progressive steps. At the time of the insult, an anterior-posterior (A/P) force is inflicted on the pelvis. This force causes an initial failure of the symphysis pubis or an initial fracture to the pubic bone. This causes the anterior portion of the pelvic ring to be separated apart. As the A/P force increases, this separation increases causing rupture first to the anterior sacro-iliac ligament followed by failure of the interosseous ligament and finally the posterior sacroiliac ligament; all three ligaments being posteriorly located in the pelvic ring. This progressive motion is thought to be one of a rotation about the sacroiliac joint (SIJ). A complete failure of the pelvic ring occurs when both sacro-iliac ligaments rupture.

The specific aim of this project is to simulate open book injury in a laboratory environment in order to better understand the mechanics of this injury. Experiments were conducted on cadavers where anterior-posterior compressive loads were applied to the pelvis. A motion tracking system was utilized to determine the changes in the kinematics of the pelvis including both sacroiliac joints.

Testing consisted of applying the load incrementally to the pelvic ring and measuring the corresponding position of the iliac bones with respect to the sacrum; this forms what is referred to as the motion data. After failure, careful dissection was conducted in order to digitize bony landmarks including the geometry of the pelvis, and the attachment locations of the different fiber bundles of the different ligamentous structures. Motion and digitization data were then combined to quantify the kinematics of the injured human pelvis using the screw displacement axis concept. Computer graphics was also

used to create a three dimensional animation of the progression of pelvis failure. The method is based on combining the geometrical data describing the topography of the pelvic articulating surfaces and the kinematics data describing the relative motions between the three bones comprising the human pelvis.

2. Experimental methods

2.1. Instrumentation

The pelvis is a ring structure uniting the trunk and the lower limbs [12,13]. It is comprised of three bones: the sacrum, and the right and left innominate iliac bones. The relative spatial motions between each pair of bones are described by three rotations and three translations. These motions were measured experimentally using the 3-SPACE Tracking and Digitizing system manufactured by the McDonnell Douglas Electronics Company. The accuracy of this system has been previously determined when it was used to measure the three-dimensional kinematics of the human wrist joint [14] and the human tibio-femoral and patello-femoral joints [15–18]. It is a true six-degree-of-freedom measurement device that allows the measurement of the translational and the rotational components of the three-dimensional relative motion between two rigid bodies. The system consists of a source that generates a low frequency electromagnetic field that is sensed by different sensors. The system is also used as a digitizer and includes a stylus that is used to designate the point to be digitized. The stylus is a handhold device that houses a magnetic field sensor. It was found that the mean maximum position error using the stylus did not exceed 0.9 mm [17].

2.2. Experimental set-up

Fresh frozen cadaveric pelvi were used in this study. Each pelvis was allowed to thaw at room temperature 24 h before testing. Careful dissection was conducted in order to isolate the pelvic ring and to remove all excessive muscles beyond the L5 level while keeping intact the ligamentous structures that provide stability to the pelvic ring. These posterior stabilizing structures form the posterior tension band of the pelvis and include the transverse and longitudinal fibers of the posterior sacroiliac ligaments, the sacrotuberous ligaments, the sacrospinous ligaments, the iliolumbar ligaments, and the anterior sacroiliac ligaments.

Each pelvis was instrumented as shown in Fig. 1 by rigidly attaching the source to the left ilium, one sensor to the anterior surface of the sacrum and another sensor to the right ilium. The symphysis pubis was then sharply disrupted. In order to simulate anteroposterior compression of the pelvis, it was positioned prone in an 1122 Instron Machine resting on four points: the two pubic tubercles and the two anterior superior iliac spines (ASIS). Loading was then applied in a direction perpendicular to the plane containing these four points that lay in a plane parallel to the frontal plane. A 36 cm × 36 cm × 18 mm thick piece of plywood was attached to the moving head of the Instron to facilitate the application of the compressive load to the sacrum, as shown in Fig. 1. Also, in order to eliminate friction from the surface where the pelvis is resting anteriorly, plastic sheets soaked with liquid soap were placed between the pelvis and the fixed base of the Instron. This allowed the symphysis pubis and the sacroiliac joints to open freely under compressive loads.

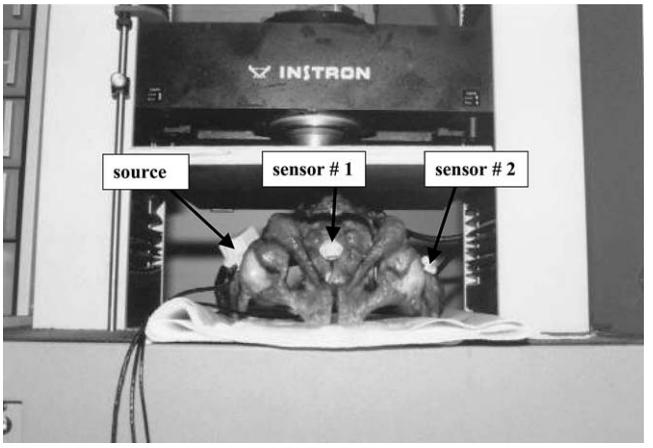

Fig. 1. Experimental set-up. The source is attached to the left ilium, sensor #1 is attached to the anterior surface of the sacrum and sensor #2 is attached to the right ilium.

During testing, the load was increased incrementally to produce incremental openings in the symphysis pubis. During this simulated open book pelvic injury, it has been observed that the anterior part of the sacroiliac ligament failed first, followed by the interosseous, and finally the posterior part. Testing was stopped when the ischial tuberosities were subjected to direct loading because at this position, loading was not applied to the sacrum. At this stage, it was observed that the left sacroiliac joint was completely disrupted while the right sacroiliac joint was opened partially. The pelvis was then unloaded, removed from the Instron, and the right SIJ was manually failed. Three tests were then conducted. The first test simulates only opening of the left SIJ. The pelvis was thus held such that both right and left SIJs were closed, and then manual external rotation was applied to the left SIJ while holding the pelvis in a supine position. The output of the 3-SPACE system was collected for different openings of the symphysis pubis until maximum opening. The second test was conducted to simulate only opening of the right SIJ by manually externally rotating the right SIJ. The third test was conducted by applying manually equal external rotations to

both joints until maximum opening, simulating thus their simultaneous openings.

Motion data consisted of the spatial position and orientation of the axes located in each of the two sensors attached to the sacrum and the right ilium, respectively, with respect to the coordinate system of axes located in the source which was attached to the left ilium, at different positions of the pelvic ring. The sacroiliac joints were disarticulated after all motion data were collected. Care was taken in order not to alter the position of the source and the sensors. In order to establish the global coordinate system of axes on the sacrum, the following landmarks were digitized: the middle of the promontory, the right and left anterior superior iliac spines, and the right and left pubic tuberosities. Digitization data describe the position and orientation of the system of axes located in the stylus sensor with respect to the source coordinate system of axes. Digitization data also include data that describes the spatial position and orientation of the system of axes located in each of the sensors attached to the bones with respect to the source coordinate system of axes during the digitization of each bony landmark in order to fully define each position of digitization.

The topology of the surfaces forming the sacroiliac joints and the interosseous sacroiliac ligaments was then measured. On these surfaces, and using a fine tip permanent black marker, grid lines were drawn 2 mm apart forming a mesh of square elements, approximately 2 mm x 2 mm, over the entire surfaces. The corner points of these elements were then digitized along with other bony landmarks including all ligamentous attachments.

3. Data analysis

3.1. Construction of sacrum bony coordinate system and coordinate transformations

Using the digitization data, the sacrum bony (global) coordinate system of axis was determined and the transformations between the source and/or each sensor and this bony system were calculated. Combining these transformations with the motion data, the relative positions between the right ilium, the left ilium and the sacrum were determined at different stages of a simulated open book fracture. In the analysis, the following sets of coordinate systems of axes were identified: a sensor coordinate system located within the source which was rigidly attached to the left ilium; two sensor coordinate systems located within the sensors which were attached to the right ilium and the sacrum, respectively. These systems of axes are shown in Fig. 2.

The sacrum (global) bony coordinate system is determined from the digitization data describing the location of the middle of the promontory, the right and left anterior superior iliac spines and the left pubic tuberosity, points O, A, B and C, respectively, in Fig. 2. The origin of this system is located at point O, the middle of the promontory. The *X*-axis is parallel to the line connecting the two anterior superior iliac spines, the positive direction being from left to right. The *Y*-axis is defined as being perpendicular to the plane containing points A, B and C; the positive direction being anterior. The third axis, the global *Z*-axis is obtained by a cross product to define a right -handed coordinate system. Hence, if $\mathbf{e}_x$, $\mathbf{e}_y$, and $\mathbf{e}_z$ are three unit vectors parallel to the (*X*, *Y*, *Z*) axes, respectively, one can write:

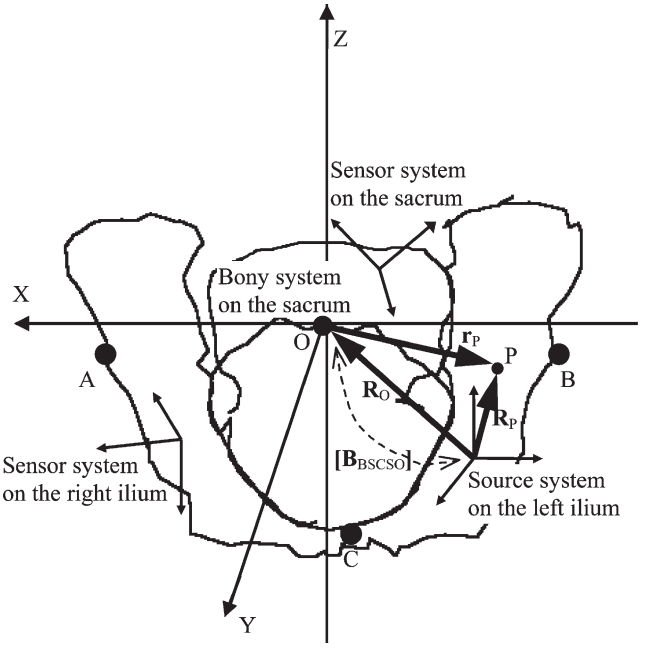

Fig. 2. Source system, two sensor systems and sacrum bony system of axes.

$$\mathbf{e}_x = (\mathbf{r}_A - \mathbf{r}_B)/|\mathbf{r}_A - \mathbf{r}_B| \quad (1)$$

where $\mathbf{r}_A$ and $\mathbf{r}_B$ are the position vectors of the right and left anterior superior iliac spines, respectively, with respect to the source coordinate system. The unit vector $\mathbf{e}_y$ is then obtained as:

$$\mathbf{e}_y = (\mathbf{e}_x \mathrm{x} \mathbf{e}_{BC})/|\mathbf{e}_x \mathrm{x} \mathbf{e}_{BC}| \quad (2a)$$

where $\mathbf{e}_{BC}$ is calculated as:

$$\mathbf{e}_{BC} = (\mathbf{r}_C - \mathbf{r}_B)/|\mathbf{r}_C - \mathbf{r}_B| \quad (2b)$$

where $\mathbf{r}_C$ is the position vector of the left pubis tuberosity with respect to the source coordinate system. Finally, $\mathbf{e}_z$, directed proximally, is obtained as the cross product of $\mathbf{e}_x$ and $\mathbf{e}_y$. The rotation matrix from the source coordinate system to the sacrum (global) bony coordinate system,

$[R_{SOBSC}]$

is thus written as:

$$[R_{SOBSC}] = [\mathbf{e}_x \ \mathbf{e}_y \ \mathbf{e}_z]^T = \begin{bmatrix} l_x & l_y & l_z \\ m_x & m_y & m_z \\ n_x & n_y & n_z \end{bmatrix}^T \quad (3)$$

where (l, m, n) are direction cosines. Consequently, the position vectors of any point in space with respect to the source coordinate system and the sacrum (global) bony coordinate system, $\mathbf{R}_P$ and $\mathbf{r}_P$, respectively, are related according to the following relation:

$$\{\mathbf{R}_P\} = [B_{SOBSC}]^{-1}\{\mathbf{r}_P\} \quad (4)$$

where $\{\mathbf{R}_P\} = [1 \ R_{Px} \ R_{Py} \ R_{Pz}]^T$, $\{\mathbf{r}_P\} = [1 \ r_{Px} \ r_{Py} \ r_{Pz}]^T$ and

$[B_{SOBSC}]^{-1}$

is a 4 x 4 transformation matrix from the sacrum (global) bony system to the source coordinate system, and is written as:

$$[B_{SOBSC}]^{-1} = \begin{bmatrix} 1 & [\mathbf{0}] \\ [R_{Ox} \ R_{Oy} \ R_{Oz}]^T & [R_{SOBSC}]^{-1} \end{bmatrix} \quad (5)$$

$$= [B_{BSCSO}]$$

where $\mathbf{R}_O = (R_{Ox}, R_{Oy}, R_{Oz})$ is the position vector of the origin of the sacrum (global) bony coordinate system with respect to the source coordinate system, and **[0]** is a null row vector of order 3. $\mathbf{R}_O$ and $[B_{BSCSO}]$, which is the transformation matrix from the sacrum (global) bony coordinate system to the source coordinate system, are shown in Fig. 2.

Fig. 3 shows the 4×4 transformation matrices from the source system to the sensors coordinate systems located on the right ilium and the sacrum, $[B_{SOSRIL}]$ and $[B_{SOSSC}]$, respectively, which are measured using the 3-SPACE system at a given instant. They are expressed in terms of the rotation matrices from the sensors coordinate systems on the right ilium and the sacrum to the source coordinate system, $[R_{SRILSO}]$ and $[R_{SSCSO}]$, respectively, and in terms of the position vectors of the origin of these two sensor systems with respect to the source system.

The transformation matrix from the global bony coordinate system (located on the sacrum) to the sensor coordinate system on the sacrum, $[B_{BSCSSC}]$ remain unchanged because these two coordinate systems are located on the same bone as shown in Fig. 3, and is obtained as follows:

$$[B_{SSCBSC}] = [B_{SOBSC}]\,[B_{SSCSO}] \quad (6)$$

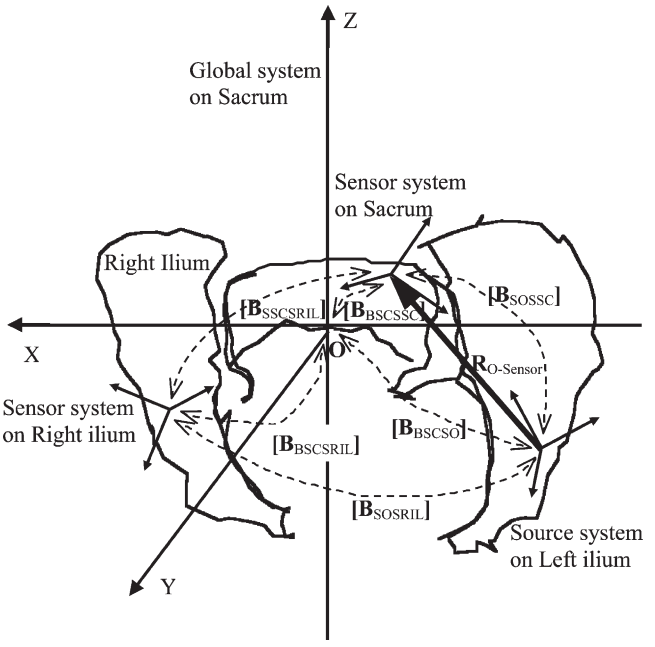

Fig. 3. Transformation matrices between the sensor coordinate systems located on the sacrum and the right ilium, the global coordinate system and the source coordinate system.

where $[B_{SSCBSC}] = [B_{BSCsSC}]^{-1}$ and $[B_{SSCSO}] = [B_{SOSSC}]^{-1}$.

In order to calculate the distances between different points on the sacrum and/or on the right and/or left ilia at any position during pelvis motion, it is necessary to calculate their coordinates with respect to the sensor and/or sacrum coordinate systems attached to their respective bones. This process includes combining the motion data and the digitization data. As an illustration, the procedure to calculate the distance between a point on the left ilium, point P_{li}, and a point on the sacrum, point P_{sc}, at a given position of the pelvis, position 2 for instance, is depicted in Fig. 4 and is described hereafter. The components of the position vector of any point, P_{li}, on the left ilium with respect to the source coordinate system, $\mathbf{r}_{li-so}$, are unchanged during the motion of the pelvis because the source is attached to the left ilium. The measured kinematics data includes the transformation matrix from the source coordinate system to the sensor coordinate system attached to the sacrum at position 2, $[B_{SOSSC}]_2$. Also, the digitization data of point P_{sc} includes the transformation matrix between the source coordinate system and the sensor coordinate system on the sacrum at the position of digitization $[B_{SOSSC}]_d$, and the coordinates of point P_{sc} with respect to the source system at the position of digitization, $(\mathbf{r}_{sc-so})_d$. Therefore, $\mathbf{r}_{sc-sc}$, which represents the position vector of point P_{sc} with respect to the sensor coordinate system on the sacrum, can be obtained as

$$\{\mathbf{r}_{sc-sc}\} = [B_{SOSSC}]_d\{\mathbf{r}_{sc-so}\}_d \quad (7)$$

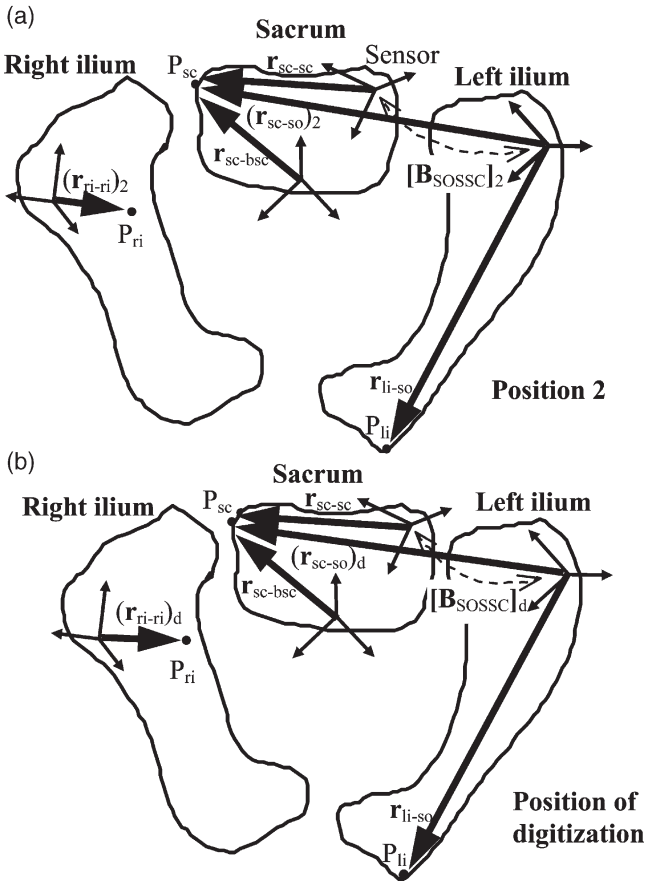

Fig. 4. Transformation matrices between source and sensor systems at an arbitrary position (position 2) and at the position of digitization.

Accordingly, the vector $(\mathbf{r}_{sc-so})_2$, which represents the position vector of point P_{sc} with respect to the source system at position 2, can be calculated as

$$\{\mathbf{r}_{sc-so}\}_2 = [B_{SOSSC}]_2^{-1}\{\mathbf{r}_{sc-sc}\} \quad (8)$$

Knowing $\mathbf{r}_{li-so}$ and $(\mathbf{r}_{sc-so})_2$, the distance between points P_{li} and P_{sc} can be calculated at position 2.

A similar procedure is used to calculate the distance between point P_{li} and point P_{ri}, which is a point on the right ilium. The coordinates of P_{ri} with respect to the source at position 2 are given as $(\mathbf{r}_{ri-so})_2$ and calculated as

$$\{\mathbf{r}_{ri-so}\}_2 = [B_{SOSRIL}]_2^{-1}\{\mathbf{r}_{ri-ri}\} \quad (9)$$

where

$$\{\mathbf{r}_{ri-ri}\} = [B_{SOSRIL}]_d\{\mathbf{r}_{ri-so}\}_d \quad (10)$$

where

$[B_{SOSRIL}]_2^{-1}$

is the transformation matrix from the sensor system on the right ilium to the source system at position 2,

$[B_{SOSRIL}]_d$

is the transformation matrix from the source system to the sensor system on the right ilium at the position of digitization, $\mathbf{r}_{ri-ri}$ is position vector of point P_{ri} with respect to the sensor coordinate system on the right ilium.

3.2. Graphical displays of pelvic ring motions

Computer graphics was used to have a better visualization of the three dimensional motions of the pelvic ring. This was accomplished by combining the kinematics data and the digitization data describing the geometry of the sacrum and both right and left ilia. Geometric data included the attachment locations of several ligaments and the locations of several bony landmarks located on the articular surfaces forming the sacroiliac joint. In order to obtain a graphical display of the pelvic motion—as shown in Fig. 5, it is necessary to calculate the coordinates of all points located on the sacrum and the right and left ilia with respect to the global system of axes (fixed to the sacrum) at all joint positions. For instance, vectors $(\mathbf{r}_{ri-bsc})_2$, $(\mathbf{r}_{li-bsc})_2$ and $(\mathbf{r}_{sc-bsc})_2$ that represent the position vectors of points P_{ri}, P_{li}, and P_{sc} located on the right ilium, left ilium and sacrum, respectively, with respect to the bony coordinate system at position 2 are given as:

$$\{\mathbf{r}_{ri-bsc}\}_2 = [B_{SSCBSC}]\,[B_{SOSSC}]_2\,\{\mathbf{r}_{ri-so}\}_2 \quad (11a)$$

$$\{\mathbf{r}_{li-bsc}\}_2 = [B_{SSCBSC}]\,[B_{SOSSC}]_2\,\{\mathbf{r}_{li-so}\}_2 \quad (11b)$$

$$\{\mathbf{r}_{sc-bsc}\}_2 = [B_{SSCBSC}]\,[B_{SOSSC}]_2\,\{\mathbf{r}_{sc-so}\}_2 \quad (11c)$$

3.3. Determination of pelvic ring's kinematics using the screw axis displacement method

The three-dimensional relative motion between two rigid bodies can be described as a rotation about and a translation along a uniquely defined axis, which is the screw displacement axis. The parameters required to

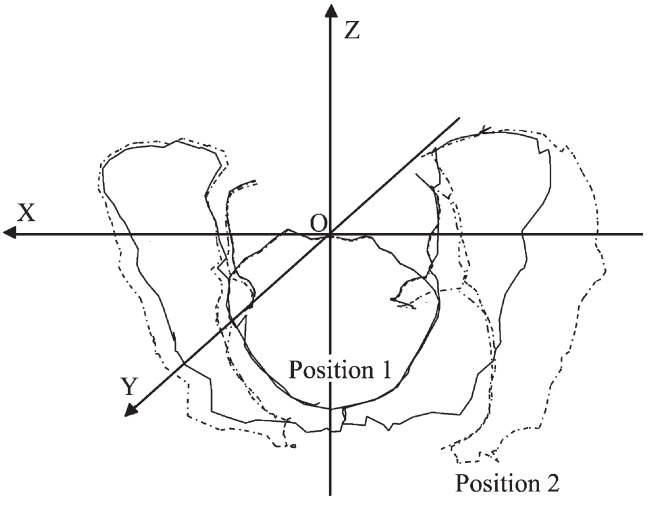

Fig. 5. Graphical display showing a pelvis at two positions.

define the general motion of a moving body—body 1—from position 1 to position 2 in terms of a screw motion include the angle of rotation about the screw axis σ, the translation along the screw axis *p*, the coordinates of any point on the screw axis (x_0, y_0, z_0), and the direction cosines (*l*, *m*, *n*) of the screw axis with respect to a system of axes attached to the fixed body [19].

The coordinates of any point located on the moving body at position 1 (x_1, y_1, z_1) are related to its coordinates at position 2 (x_2, y_2, z_2) according to the following relation:

$$[1 \;\; x_2 \;\; y_2 \;\; z_2]^{\mathrm{T}} = [\mathrm{B}]_{1-2}[1 \;\; x_1 \;\; y_1 \;\; z_1]^{\mathrm{T}} \tag{12}$$

where

$$[\mathrm{B}]_{1-2} = \begin{bmatrix} 1 & 0 & 0 & 0 \\ pl - x_0V(-1 + l^2) & & & \\ -y_0(-Sn + Vlm) & C + Vl^2 & -Sn + Vlm & Sm + Vlm \\ -z_0(Sm + Vnl) & & & \\ pm - x_0(Sn + Vlm) & & & \\ -y_0V(-1 + m^2) & Sn + Vlm & C + Vm^2 & -Sl + Vmn \\ -z_0(-Sl + Vmn) & & & \\ pn - x_0(Sm + Vnl) & & & \\ -y_0(-Sl + Vmn) & -Sm + Vnl & Sl + Vmn & C + Vn^2 \\ -z_0V(-1 + n^2) & & & \end{bmatrix} \tag{13}$$

where $V = 1 - \cos\sigma$, $S = \sin\sigma$ and $C = \cos\sigma$.

For our purpose, body 1 (moving body) is the right ilium or the left ilium, and body 2 (fixed body) is the sacrum. Motion data and geometric data are combined to calculate $[\mathrm{B}_{1-2}]_1$ and $[\mathrm{B}_{1-2}]_2$, which are the transformation from body 1 (left or right ilium) to body 2 (sacrum) at positions 1 and 2, respectively. The motion of body 1 from position 1 to position 2 can thus be described by a transformation matrix $[\mathrm{B}]_{1-2}$, which is calculated as:

$$[\mathrm{B}]_{1-2} = [\mathrm{B}_{1-2}]_2^{-1}[\mathrm{B}_{1-2}]_1 \tag{14}$$

The parameters of the screw axis describing the motion of body 1 (right or left ilium) from position 1 to position 2 with respect to body 2 (sacrum) are thus calculated by equating Eqs. (13) and (14).

3.4. Determination of the best-fit planes describing the sacroiliac articular surfaces

Visual inspection of the dissected pelvi revealed that the sacroiliac articular surfaces are almost parallel to the sagittal plane, the *yz* plane. Therefore, these surfaces were mathematically represented using the plane equation:

$$x = \mathrm{A}y + \mathrm{B}z + \mathrm{C} \tag{15}$$

The constants A, B and C describing the planar approximation of each surface were determined using the least square method to find the best-fit plane that contains a certain number of digitized points, n, located on that surface. The angles between each planar surface and the sagittal, frontal and transverse planes, α, β and γ, respectively, were then calculated using the following relations:

$$\gamma = \cos^{-1}\left(\frac{|-\mathrm{B}|}{\sqrt{1 + \mathrm{A}^2 + \mathrm{B}^2}}\right) \tag{16}$$

$$\alpha = \cos^{-1}\left(\frac{1}{\sqrt{1 + A^2 + B^2}}\right)$$

$$\beta = \cos^{-1}\left(\frac{|-A|}{\sqrt{1 + A^2 + B^2}}\right)$$

Finally, and in order to have a better visualization of the kinematics of the pelvic ring during a simulated open book fracture, the relative positions of each screw axis with respect to each of these planar surfaces were calculated.

4. Results

4.1. Geometry of the articular surfaces

Results were obtained from two (2) cadavers: pelvis #1 was obtained from a male donor while pelvis #2 was obtained from a female donor. Figs. 6 and 7 show a graphical display of each intact pelvic ring, respectively. Each figure includes a frontal view (X–Z plane), a sagittal view (Y–Z plane) and a transverse view (X–Y plane)

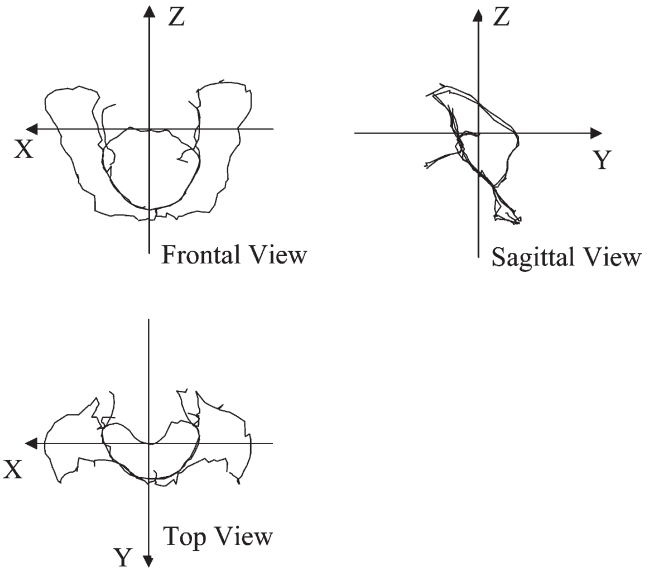

Fig. 6. Three orthogonal views of the pelvic ring for pelvis #1 (male).

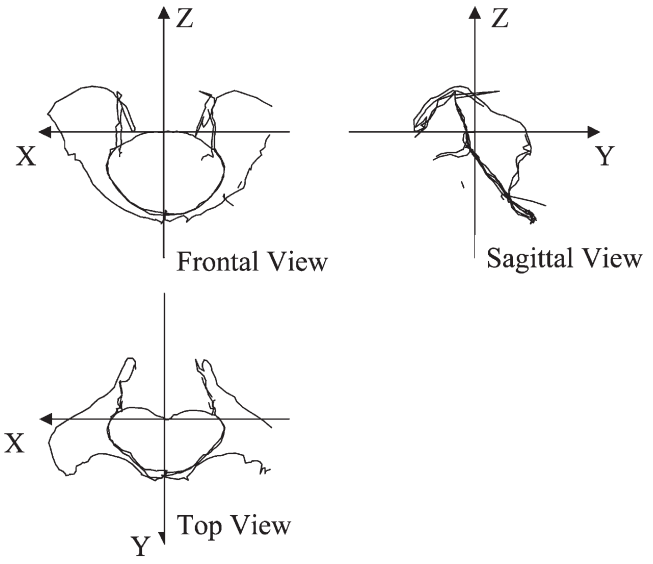

Fig. 7. Three orthogonal views of the pelvic ring for pelvis #2 (female)

of the left and right hipbones and the sacrum including the sacroiliac joint lines. Digitization data were used to construct these figures. For pelvis #1, the data shown in Fig. 6 consists of 232 digitized points which include 15 points located on the right sacroiliac joint line, 17 points on the left sacroiliac joint line, and 17 points on the promontory and ala of the sacrum which form the posterior border of the pelvic inlet, 93 points on the periphery of the left hip bone, and 90 points on the periphery of the right hip bone. For pelvis #2, the data shown in Fig. 7 consists of 251 digitized points which include 13 points located on the right sacroiliac joint line, 13 points on the left sacroiliac joint line, and 19 points on the promontory and ala of the sacrum which form the posterior border of the pelvic inlet, 100 points on the periphery of the left hip bone, and 106 points on the periphery of the right hip bone. Figs. 6 and 7 show that the pelvic inlet of the female pelvis is larger than that of the male pelvis, especially in the anteroposterior diameter.

Figs. 8 and 9 show sagittal views of digitized points located on the iliac surfaces of the sacroiliac joints. These include an anteroinferior part forming the articular surface of the sacroiliac joint and a posterosuperior part forming the attachment surface for the interosseous sacroiliac ligaments. Fig. 8a shows 140 points that were digitized on the iliac articular surface of the left sacroiliac joint and 82 points on the iliac attachment surface for the left interosseous ligament for pelvis #1. Fig. 8b shows 178 points that were digitized on the iliac articular surface of the left sacroiliac joint and 97 points on the iliac attachment surface for the left interosseous ligament for pelvis #2. Fig. 9a shows 102 points that were digitized on the iliac articular surface of the right sacroiliac joint and 99 points on the iliac attachment surface for the right interosseous ligament for pelvis #1. Fig. 9b

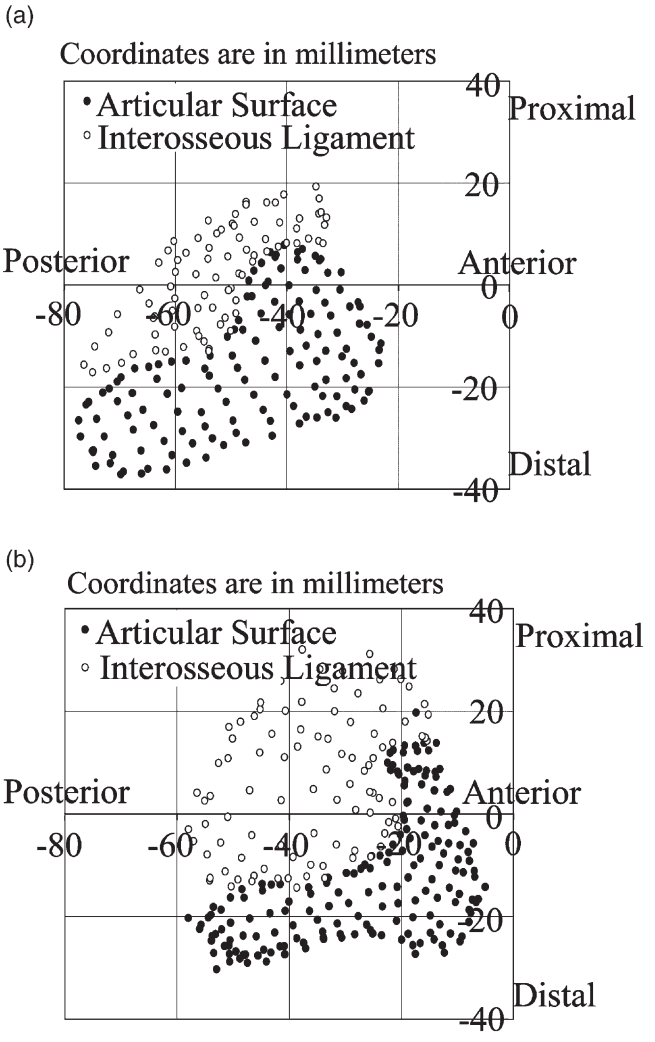

Fig. 8. Digitized points located on the left iliac surface defining the sacroiliac articular surface and the attachment site of the interosseous ligament. (a) Pelvis #1 (b) Pelvis #2.

shows 142 points that were digitized on the iliac articular surface of the right sacroiliac joint and 78 points on the iliac attachment surface of the right interosseous ligament for pelvis #2.

4.2. Correlation between symphysis pubis opening and sacroiliac joint opening

Data were collected to simulate three types of joint opening: opening of the right SIJ only, opening of the left SIJ only, and the simultaneous opening of both right and left SIJ's. At each position of the pelvis during each of these simulations, the right and left sacroiliac joint openings, the symphysis pubis opening, and the distance between the right and left anterior superior iliac spines (ASIS's) were calculated.

Figs. 10–14 show the variations in the transverse, vertical and anterior components of the symphysis pubis opening vector. These three quantities represent the

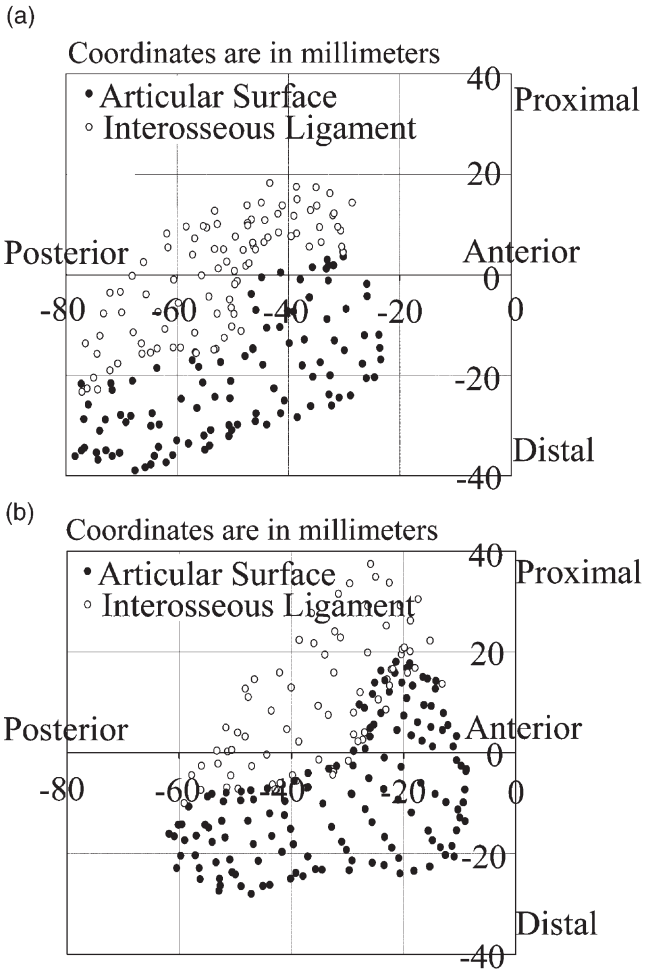

Fig. 9. Digitized points located on the right iliac surface defining the sacroiliac articular surface and the attachment site of the interosseous ligament. (a) Pelvis #1 (b) Pelvis #2.

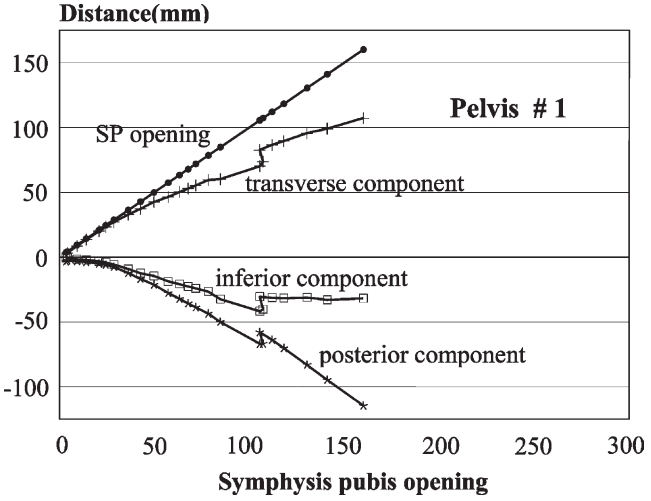

Fig. 10. Variations in the components of the symphysis pubis (SP) opening during isolated opening of the right SIJ for pelvis #1.

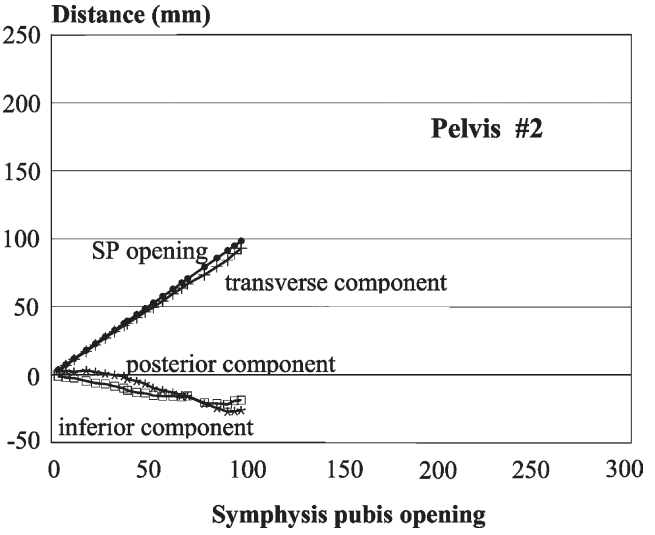

Fig. 11. Variations in the components of the symphysis pubis (SP) opening during isolated opening of the right SIJ for pelvis #2.

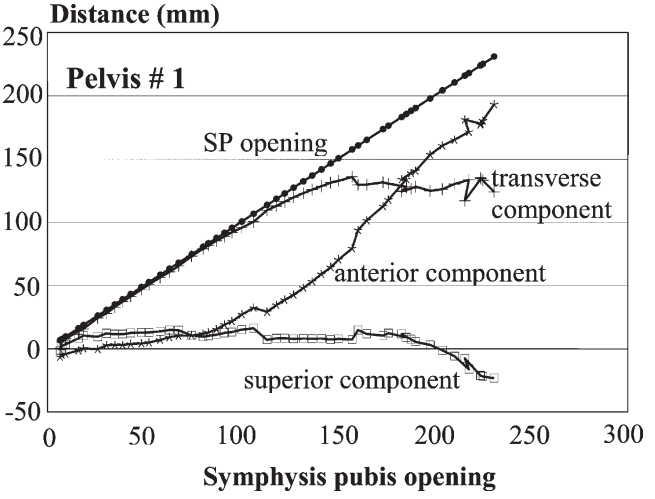

Fig. 12. Variations in the components of the symphysis pubis (SP) opening during isolated opening of the left SIJ for pelvis #1.

components of the position vector of the right symphysis pubis with respect to the left symphysis pubis as origin. The results show that when only the right SIJ was opened while the left SIJ was kept closed, the right pubic bone moved posterior and inferior to the left pubic bone as shown in Figs. 10 and 11 for pelvis #1 and pelvis #2, respectively. This trend was reversed when only the left SIJ was opened and the right SIJ was kept closed; the symphysis pubis opening vector was found to have an anterior and superior component at all joint positions as shown in Fig. 12 for pelvis #1. This indicates that the left pubic bone moved posterior and inferior to the right pubic bone.

When both SIJ joints were opened simultaneously, Figs. 13 and 14 show that the symphysis pubis opening did not have a vertical component. In this case, and up

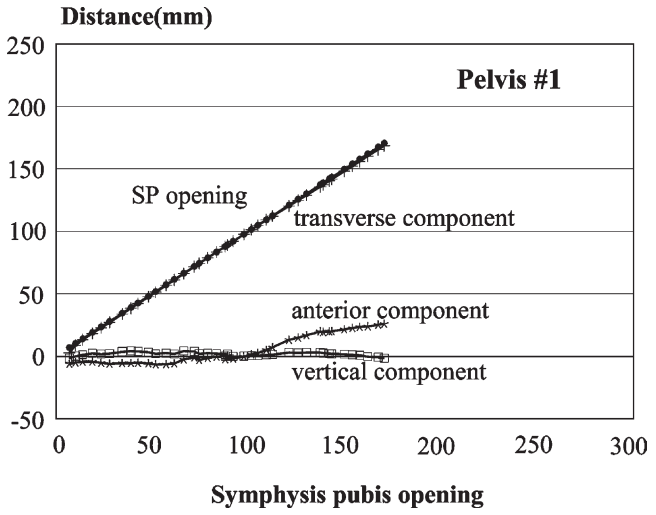

Fig. 13. Variations in the components of the symphysis pubis (SP) opening during the simultaneous opening of the right and left SIJ's for pelvis #1.

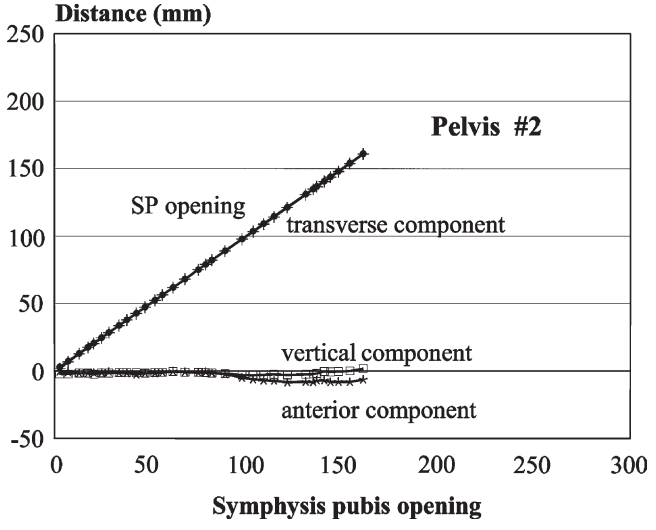

Fig. 14. Variations in the components of the symphysis pubis (SP) opening during the simultaneous opening of the right and left SIJ's for pelvis #2.

to 100 mm of symphysis pubis opening, also the anterior component was negligible. This was expected since a symmetric motion occurred when both joints were opened simultaneously. When the symphysis pubis opening exceeded 100 mm, a small anterior component was identified, but most of the opening was in the transverse direction.

Calculations have shown that the distance between the right and left ASISs was almost the same during the three simulations when the symphysis pubis opened up to 50 mm. At 50 mm opening, the distance between the two ASISs was 263 mm during the simulation of an opening of only the right SIJ in pelvis #1 and pelvis #2; this distance was 264 mm and 258 mm in pelvis #1 and pelvis #2, respectively, when only the left SIJ was opened, and 263 mm in both pelvi when both joints were opened simultaneously.

As the opening of the symphysis pubis increased, the distance between the two ASISs was slightly higher when both joints were opened simultaneously than when one joint was opened, keeping the other joint closed. For pelvis #1, this distance was 315 mm when the symphysis pubis opening reached a maximum allowable opening of 162 mm with only the right SIJ was opened. When both SIJ's were opened simultaneously, the symphysis pubis opened a maximum of 170 mm and the corresponding distance between the two ASISs was 338 mm. In pelvis #2, the values for the maximum opening of the symphysis pubis were 100, 70 and 162 mm when a right opening, a left opening and a simultaneous opening were simulated, respectively. The corresponding distances between the two ASISs were 288, 270, and 317 mm, respectively.

Figs. 15 and 16 show the relationships between SIJ openings and symphysis pubis opening for pelvis #1 when only the right SIJ was opened, and when both joints were opened simultaneously, respectively. Fig. 15 shows that in pelvis #1, the symphysis pubis opening reached a maximum of 162 mm when only the right SIJ was opened to a maximum of 63 mm. Fig. 15 shows that when both joints were opened simultaneously, the symphysis pubis opening reached a maximum of 170 mm; the corresponding openings of the right and left SIJ's were 33 and 50 mm, respectively. Similar results were obtained from pelvis #2 where the symphysis pubis opening reached a maximum of 100 mm when the right SIJ was opened to a maximum of 20 mm, and a maximum of 70 mm when the left SIJ was opened to a maximum of 15 mm, respectively. When both joints were opened simultaneously, the symphysis pubis open-

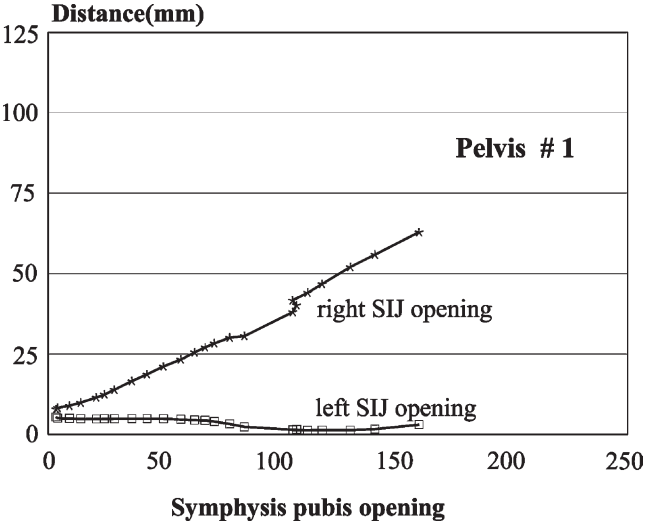

Fig. 15. Relationships between symphysis pubis opening and SIJ openings during isolated opening of the right SIJ for pelvis #1.

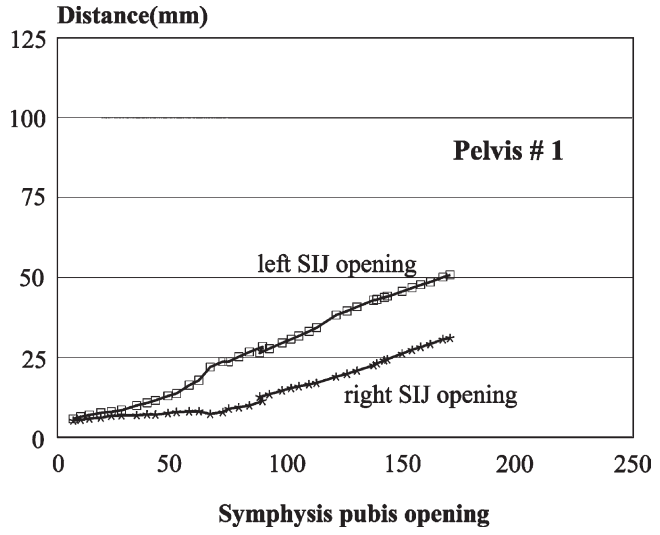

Fig. 16. Relationships between symphysis pubis opening and SIJ openings during the simultaneous opening of the right and left SIJ's for pelvis #1.

ing in pelvis #2 reached a maximum of 162 mm; both right and left SIJ's opened to 20 mm each.

4.3. Best-fit planar approximations of the surfaces of the sacroiliac joints

Figs. 17a and 17b show the best fit planes that approximate the articular surfaces of the sacroiliac joints for pelvis #1 and pelvis #2, respectively. Each of these planes is defined using the following mathematical relation ($x = A\,y + B\,z + C$) where the constants A, B and C are given in Table 1. In this equation, x, y and z are in millimeters. The angles α, β and γ that each of the best-fit planes makes with the sagittal plane, frontal plane, and transverse plane, respectively, were also calculated and are listed in Table 2. Figs. 17a and 17b also include the digitized points that define the articular surfaces.

The data presented in Tables 1 and 2 show that the two planes that approximate the right and left articular surfaces of the sacroiliac joints were almost symmetric with respect to the sagittal plane. The relative spatial orientations of these planes were almost identical in the two pelvi that were tested, and were directed from proximal and lateral to distal and medial and from posteromedial to anterolateral. The average angles that these best-fit planes made with the transverse plane, sagittal plane and frontal plane were 80.7 degrees (± 4.60), 15.7 degrees (± 3.3) and 77.8 degrees (± 1.1), respectively.

4.4. Screw displacement axes

Screw displacement axes data describing the motions that occur during the isolated and simultaneous opening of the right and left sacroiliac joints for pelvis #1 and

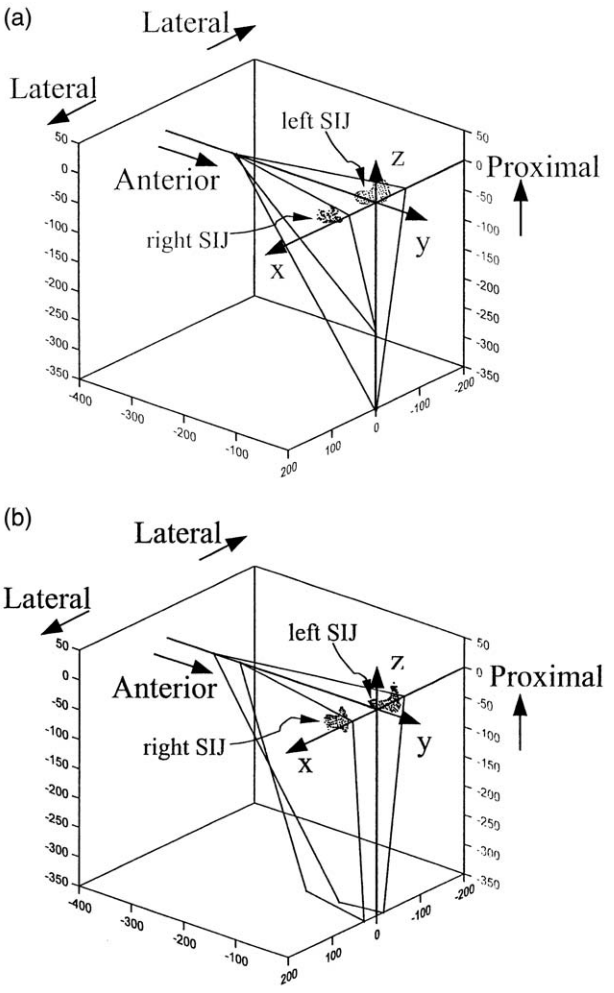

Fig. 17. Best Fit Planes approximating the right and left sacroiliac articular surfaces along with the defining digitized points (a) Pelvis #1 (b) Pelvis #2.

pelvis #2 are listed in Tables 3–6. Tables 3 and 4 show the data for pelvis #1 and Tables 5 and 6 show the data for pelvis #2. Tables 3 and 5 describe the screw axes during the isolated opening of the right and left joints, while Tables 4 and 6 describe the screw axes during the simultaneous opening of both joints.

In what follows, a description of the data included in Tables 3–6 is presented. Each screw axis describes the motion between two consecutive positions that are listed in the second column. In Table 3, axis a and axis 1 are the screw axes that describe the motions between positions 1 and 2 for each of the left and right sacroiliac joints, respectively; axes b and 2 describe the motions between positions 2 and 3, and so forth. The third column includes two angles, ϕ_1 and ϕ_2, where ϕ_1 is the angle of rotation between the two consecutive positions listed in the second column and ϕ_2 is the angle of rotation between the initial position and the second of these two consecutive positions. For instance, in Table 3, the second entry from the top in the third column indicates

Table 1
Coefficients defining the equations of the best fit planes ($x = Ay + Bz + C$) approximating the left and right sacroiliac articular surfaces for pelvis #1 and pelvis #2

	A		B		C	
	Pelvis #1	Pelvis #2	Pelvis #1	Pelvis #2	Pelvis #1	Pelvis #2
Right articular surface	0.23	0.22	0.28	0.08	63.69	57.82
Left articular surface	–0.24	–0.19	–0.18	–0.13	–64.39	–59.44

Table 2
Angles in degrees between the best fit planes approximating the sacroiliac articular surfaces and the sagittal (α), frontal (β) and transverse (γ) planes for pelvis #1 and pelvis #2

	α (deg)		β (deg)		γ (deg)	
	Pelvis #1	Pelvis #2	Pelvis #1	Pelvis #2	Pelvis #1	Pelvis #2
Right articular surface	19.92	13.18	77.51	77.63	74.74	85.53
Left articular surface	16.7	12.96	76.71	79.33	80.07	82.72

Table 3
Parameters defining the screw displacement axes describing the motions that occur during the isolated opening of the left and right sacroiliac joints for pelvis #1. Angles are in degrees

	Position	ϕ_1/ϕ_2	p(mm)	θ_l	θ_{Tl}	θ_x	θ_y	θ_z	α	β	γ
Axis a	1–2	11.6/11.6	–0.71	10.5	–	63.5	57.8	44.0	26.5	32.2	46.1
Axis b	2–3	8.4/19.4	–0.91	15.1	–	80.9	79.1	14.3	9.1	10.9	75.8
Axis c	3–4	13.2/31.1	–0.18	17.1	–	86.2	82.1	8.8	3.8	7.9	81.2
Axis d	4–5	10.2/39.5	1.03	27.4	–	75.3	78.1	19.1	14.7	12.0	70.9
Axis e	1–5	39.5/39.5	0.42	0.1	–	79.4	87.7	10.9	10.7	2.3	79.2
Axis 1	1–2	11.6/11.6	0.48	–	2.1	73.4	72.3	24.7	16.6	17.8	65.4
Axis 2	2–3	10.1/21.5	0.66	–	15.9	57.3	79.3	34.9	32.8	10.7	55.0
Axis 3	3–4	12.3/31.2	0.81	–	10.3	59.0	79.7	33.0	31.0	10.4	57.0
Axis 4	4–5	11.7/42.7	1.92	–	10.8	55.1	84.5	35.5	35.0	5.5	54.5
Axis 5	1–5	42.7/42.7	4.06	–	10.9	60.8	77.3	32.4	29.2	12.7	57.7

Table 4
Parameters defining the screw displacement axes describing the motions that occur during the simultaneous opening of the left and right sacroiliac joints for pelvis #1. Angles are in degrees

	Position	ϕ_1/ϕ_2	p(mm)	θ_l	θ_{Tl}	θ_x	θ_y	θ_z	α	β	γ
Axis a	1–2	10.9/10.0	0.08	1.4	–	72.2	48.9	46.5	17.9	41.2	43.5
Axis b	2–3	9.6/19.9	–0.02	14.7	–	88.8	68.5	21.6	1.2	21.5	68.5
Axis c	3–4	10.4/29.8	–0.02	1.8	–	78.0	79.1	16.3	12.0	10.9	73.7
Axis d	4–5	9.1/38.7	–0.53	8.2	–	69.4	74.7	26.1	20.6	15.3	63.9
Axis e	5–6	11.4/49.7	–0.82	11.2	–	63.6	81.9	27.8	26.4	8.1	62.2
Axis f	6–7	8.7/58.3	–0.09	4.0	–	71.7	70.2	27.6	18.4	19.9	62.5
Axis g	1–7	58.3/58.3	–2.42	4.4	–	71.2	69.7	28.2	18.8	20.3	61.8
Axis 1	1–2	11.1/11.1	0.95	–	9.1	61.2	63.7	40.9	28.8	26.4	49.1
Axis 2	2–3	8.3/19.2	0.18	–	1.1	71.0	74.3	25.1	19.0	15.7	65.0
Axis 3	3–4	10.5/29.6	0.19	–	0.7	71.5	71.1	27.0	18.5	18.9	63.1
Axis 4	1–5	29.6/29.6	1.33	–	4.0	66.9	69.8	31.5	23.1	20.2	58.5

Table 5
Parameters defining the screw displacement axes describing the motions that occur during the isolated opening of the left and right sacroiliac joints for pelvis #2. Angles are in degrees

	Position	ϕ_1/ϕ_2	p(mm)	θ_l	θ_{Tl}	θ_x	θ_y	θ_z	α	β	γ
Axis a	1–2	10.7/10.7	–0.4	8.7	–	88.6	73.2	16.8	1.4	16.8	73.2
Axis b	2–3	11.3/21.9	–1.0	0.8	–	80.1	72.9	19.9	9.9	17.1	70.0
Axis c	3–4	9.9/31.6	–0.8	0.3	–	67.5	71.5	29.9	22.6	18.5	60.1
Axis d	1–4	31.6/31.6	–2.3	0.3	–	79.2	71.1	22.0	10.8	18.9	67.4
Axis 1	1–2	11.2/11.2	–0.1	–	5.0	77.1	74.3	20.6	12.9	15.7	68.5
Axis 2	2–3	10.6/21.7	1.0	–	13.2	68.2	65.6	33.7	21.18	24.4	56.4
Axis 3	3–4	12.5/34.1	0.3	–	3.4	78.1	72.7	21.2	11.9	17.3	65.9
Axis 4	4–5	7.5/41.3	0.3	–	8.8	88.7	75.0	15.1	1.3	15.0	75.0
Axis 5	1–5	41.3/41/3	1.4	–	4.4	77.3	72.5	21.9	12.7	17.5	68.2

Table 6
Parameters defining the screw displacement axes describing the motions that occur during the simultaneous opening of the left and right sacroiliac joints for pelvis #2. Angles are in degrees

	Position	ϕ_1/ϕ_2	p(mm)	θ_l	θ_{Tl}	θ_x	θ_y	θ_z	α	β	γ
Axis a	1–2	10.1/10.1	–0.7	1.3	–	77.8	68.0	25.4	12.2	22.2	64.5
Axis b	2–3	9.9/20.0	–0.7	3.6	–	73.0	66.9	29.3	17.0	23.1	60.7
Axis c	3–4	11.1/31.0	–0.8	2.8	–	77.7	72.0	22.1	12.3	18.0	68.1
Axis d	1–4	31.0/31.0	–2.1	3.2	–	79.0	69.1	25.6	14.0	20.9	64.6
Axis 1	1–2	9.4/9.4	–0.1	–	8.4	73.4	73.6	23.7	16.6	16.4	66.1
Axis 2	2–3	12.0/21.3	1.4	–	1.4	79.6	73.0	20.1	10.4	17.0	69.8
Axis 3	3–4	8.2/29.5	0.5	–	10.4	71.2	70.3	27.9	18.9	19.8	60.9
Axis 4	4–5	9.8/39.2	0.1	–	4.2	83.2	72.2	19.2	6.8	17.8	70.8
Axis 5	1–5	39.2/39.2	1.9	–	4.4	77.4	72.7	21.6	12.6	17.3	68.2

that a rotation of 8.4 degrees occurred about axis b as the left joint was moved from position 2 to position 3. This entry also indicates that a rotation of 19.4 degrees occurred as the left joint was moved from the initial position, position 1, to position 3. Axes e and 5 in Table 3 represent the average screw axes from the initial position, position 1, to the final position, position 5, for each of the left and right sacroiliac joints, respectively. Therefore, the values of ϕ_1 and ϕ_2 for axis e are equal to each other, both having a value of 39.5 degrees. The fourth column in these tables lists the values of the translations along the screw axis, the pitch p in millimeters, as the pelvis was moved between the two consecutive positions listed in the second column. The angles that each screw axis makes with the global x axis, y axis, z axis, yz plane (sagittal plane), xz plane (frontal plane) and xy plane (transverse plane), respectively are listed in the last six columns as θ_x, θ_y, θ_z, α, β and γ. The angles that each screw axis makes with the best-fit planes approximating the left and right articular surfaces are listed as θ_{l1} and $\theta_{r1,}$ respectively.

The results listed in Tables 3–6 indicate that the motions that occur during the isolated and simultaneous opening of the right and/or left sacroiliac joints are almost pure rotational motions. This is demonstrated by the small value for the pitch p. These results also show that the axis of rotation changes orientation with the progressive of joint opening. The average screw axis was found to be almost parallel to the plane approximating the articular surface. For instance, Table 5 shows that for pelvis #2, the angles between these axes and these planes were 0.3° and 4.4° during isolated opening of the left and right sacroiliac joints, respectively. On average the angle was found to be 4° (8 cases).

5. Discussion and conclusion

Open book injury is a common anteroposterior injury of the pelvis that is often encountered in motor vehicle accidents. This injury is usually associated with increased risk of bleeding from the pelvic vessels. Understanding the mechanism and prompt diagnosis of this injury in the emergency room are crucial to its management.

The results obtained from this study are limited because only two pelvi were tested. However, these limited data can help in understanding the correlation between SIJ disruption and the degree and direction of the symphysis pubis opening following open book injury. The results indicate that there is a direct positive correlation between the opening of the symphysis pubis

and the opening of the sacroiliac joint during open book injury. Theoretically, one may thus conclude that the extent of injury of the sacroiliac joint can be estimated from the degree of opening of the symphysis pubis as demonstrated on anteroposterior x-rays. However, due to the recoil of the pelvis after sustaining the injury, the degree of the sacroiliac joint injury will be underestimated from the x-rays.

The screw displacement axis method was also used to describe the motions that occur at the sacroiliac joints during the open book injury. The results indicate that the motion of the hipbone with respect to the sacrum on the side of the sacroiliac joint opening is almost a pure rotation because the translation was negligible along each screw axis that describes the motion between two consecutive positions. This can be translated clinically on the anteroposterior x-rays as pure opening of the sacroiliac joint without vertical displacement. Results also show that the pubic bone on the side of sacroiliac joint opening displaced inferiorly and posteriorly. The inferior displacement can be demonstrated on anteroposterior x-rays of the pelvis.

The results describing the topology of the sacroiliac joints indicate that the articular surfaces can be approximated as planar surfaces. The combination of the spatial orientation of these best fit planes and the screw axes provide an explanation for the direction of displacement of the pubic bones during open book pelvic injury. These planes are directed from proximal and lateral to distal and medial and from posteromedial to anterolateral. Fig. 18 shows the spatial location and orientation of the average screw axis during the isolated opening of the left SIJ for pelvis #2. This figure also shows all points located on the left SIJ including the articular and interosseous surfaces. The average screw axis in the sagittal view is directed obliquely from posteroinferior to anterosuperior, and in the frontal view from inferomedial to superolateral. As the joint opens anteriorly, the iliac site of the articular surface of the left SIJ moves posteriorly as appreciated from the frontal view. This view shows the projection of the screw axis and indicates that all points on the SIJ will have a displacement component that is perpendicular to the frontal plane and directed posteriorly (motion around screw axis). At the same time, and while the iliac site of the SIJ moves superiorly (as appreciated from the transverse view), the pubic bone moves inferiorly. Thus, the whole left hip bone, as one unit, opens inferiorly and laterally causing the left pubic bone to appear displaced inferiorly on the anteroposterior x-ray of a pelvis with left sacroiliac joint disruption. This inferior displacement of the pubic bone is not accompanied by sacroiliac joint translation in contrast to the vertical shear injury.

The present work describes the response of the pelvis under compressive anterior–posterior compressive loads. It is hard to compare our results with those available in the literature since only a few studies have been published to describe the biomechanics of the pelvis. These few studies either were limited to normal motions or simulated different loading conditions including side

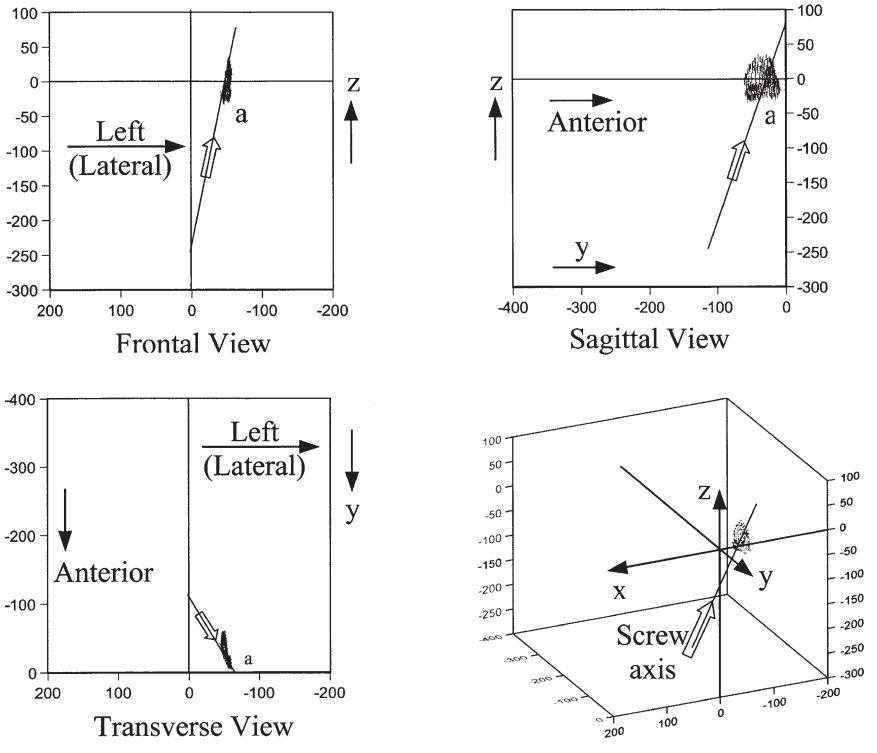

Fig. 18. Spatial location and orientation of the average screw axis during the isolated opening of the left SIJ for pelvis #2.

impact [5,6], and lateral loading [7,8]. Several authors described sacroiliac normal joint motion as a rotary motion or a rotary motion associated with translation, and proposed different axes of rotations using different underlying principles. Wilder, et al. [20] analyzed the motion permitted by the topography of the sacro-iliac joint surface. They used a Copycat Contour Gage, which is a contour follower, to establish the contour of the articular surface in the sagittal and frontal planes (slices obtained from sectioning the joint surface) at the level of Bonnaire's tubercle. A best-fit circle was then determined to best fit the contour slice. In their analysis, Wilder, et al. [20] considered the motion to be confined to one plane, and assumed the center of curvature as the axis of rotation, stating that this is possible since the articular surfaces closely conform to each other. We cannot compare our results describing the locations of the axis of rotation to those available in the literature because the former describe the kinematics of the sacroiliac joint following open book injury, while the latter correspond to normal motions in intact joints. It is also hard to compare our results describing the topology of the articular surfaces of the sacroiliac joint as best fit planes with those of Wilder, et al. [20] since they describe the contour of only one slice. Furthermore, they did not report the value of the radius of the best-fit circle approximating this slice.

In summary, it can be then concluded that in open book pelvic injuries, the pubic bone on the side of injury displaces inferiorly and the sacroiliac joint does not displace vertically on the anteroposterior x-rays. This is important since the initial assessment of the open book injury in the emergency room includes anteroposterior projection x-rays. From this study, the vertical displacement of the pubic bones on the anteroposterior x-rays can help the orthopedic surgeon in differentiating this type of injury from vertical shear injuries. Each injury is managed in a different manner. In open book pelvic injury, the sacroiliac joint is not vertically displaced in contrast to the vertical shear injury. Furthermore, the pubic bone on the side of injury will displace inferiorly, in contrast to the superior displacement that occurs in vertical shear injuries.

References

[1] Tile M. Fractures of the pelvis and acetabulum., 2nd ed & Wilkins: Williams, 1995.

[2] Drerup B, Hierholzer B. Movement of the human pelvis and displacement of related anatomical landmarks of the bony surface. J Biomech 1987;20(10):971–7.

[3] Gautsch TL, Johnson EE, Seeger LL. True three dimensional strereographic display of 3D reconstructed CT scans of the pelvis and acetabulum. Clin Orthop Rel Res 1994;305:138–51.

[4] Major NM, Helms CA. Pelvic stress injuries: the relationship between osteitis pubis stress injury) and sacroiliac abnormalities in athletes. Skeletal Radiol 1997;26:711–7.

[5] Nusholtz G, Alem N, Melvin J. Impact response and injury of the pelvis. Proceedings of the 26th STAPP Car Crash Conference 1982, no. 821160. Society of Automotive Engineers.

[6] Cesari D, Ramet M, Chair P. Evaluation of pelvic fracture tolerance in side impact. Proceedings of the 24th STAPP Car Crash Conference 1980, no. 801306. Society of Automotive Engineers.

[7] Renaundin F, Guillemot H, Lavaste F, Skalli W. A 3D finite element model of pelvis in side impact. Proceedings of the 37th STAPP Car Crash Conference 1993, no. 933130. Society of Automotive Engineers.

[8] Dawson JM, Khmelniker BV, McAndrew MP. Analysis of the structural behaviour of the pelvis during lateral impact using the finite element method. Accident Analysis and Prevention 1999;31:109–19.

[9] Hoek van Dijke GAH, Snijders CJ, Stoeckart R, Stam HJ. A biomechanical model on muscle forces in the transfer of spinal load to the pelvis and legs. J Biomech 1999;32:927–33.

[10] Judet R, Judet J, Letournel E. Fractures of the Acetabulum. Classification and Surgical Approaches for Open Reduction. J Bone Joint Surg 1964;46A:1615.

[11] Young JWR, Burgess AR. Radiological management of pelvic ring fractures: systemic radiographic diagnosis. Baltimore, MD: Urban & Schwarzenberg, 1987.

[12] Crouch JE. Functional human anatomy., 4th ed. Philadelphia, PA: Lea & Febiger, 1985.

[13] Wilson DB, Wilson WJ. Human anatomy. Oxford University Press, 1978.

[14] Jackson WT, Hefzy MS, Guo H. Determination of wrist kinematics using a magnetic tracking device. J Biomed Eng 1994;16(2):123–33.

[15] Hefzy MS, Saddemi SR, Cheng G, Hoeflinger M, Milem C. Frogameni, A.A., biomechanical comparison between high tibial osteotomy (HTO) and combined HTO and fibular osteotomy. J Clin Biomech 1994;9(5):284–90.

[16] Hefzy MS, Yang H. A three-dimensional anatomical model of the human patello - femoral joint for the determination of patello - femoral motions and contact characteristics. J Biomed Eng 1993;15:289–302.

[17] Zoghi M, Hefzy MS, Jackson WT, Fu KC. A three-dimensional morphometrical study of the distal human femur. J Eng Med 1992;206:147–57.

[18] Hefzy MS, Jackson WT, Saddemi SR, Hsieh YF. Effects of tibial rotations on patellar tracking and patello-femoral contact areas. J Biomed Eng 1992;14:329–43.

[19] Suh CH, Radcliff CW. Kinematics and mechanism design. John Wiley and Sons, 1978.

[20] Wilder DG, Pope MH, Frymoyer JW. The functional topography of the Sacroiliac Joint. Spine 1980;5(6):575–9.